Acta Oceanol. Sin., 2025, Vol. 44, No. 3, P. 71–83
https://doi.org/10.1007/s13131-025-2476-2

Seasonal variations of ocean-to-ice heat flux in north of the Fram Strait, Arctic Ocean

Yuang Liu[1], Xiaoqiao Wang[2, 3*], Jinfeng Ding[2, 3], Lujun Zhang[1]

[1] School of Atmospheric Sciences, Nanjing University, Nanjing 210023, China
[2] College of Meteorology and Oceanography, National University of Defense Technology, Changsha 410073, China
[3] Key Laboratory of High Impact Weather (Special), China Meteorological Administration, Changsha 410118, China

Received 9 December 2024; accepted 24 March 2025
© Chinese Society for Oceanography and Springer-Verlag GmbH Germany, part of Springer Nature 2025

Abstract
As the Arctic undergoes rapid warming and sea ice continues to decline, Ocean-to-Ice Heat Flux (OIHF) plays a crucial role in regulating sea ice dynamics. This study investigates the seasonal variations in ocean-to-ice heat flux in north of the Fram Strait using the regional Arctic Ocean/sea ice reanalysis product from 1991 to 2020. The analysis reveals that the OIHF exhibits significant seasonal variability, with a pronounced peak during winter in north of the Fram Strait, driven by inflows of Atlantic water. Warm Atlantic water intrusion begins in October, reaches its peak in January and February, and results in a delayed increase in OIHF, with maximum flux observed 2−3 months later. These results highlight the significant role of Atlantic water inflows in influencing Arctic sea ice dynamics and emphasize the need for further investigation into the coupled ocean-atmosphere processes that govern seasonal fluctuations in OIHF.

Key words Arctic Ocean, Ocean-to-Ice Heat Flux (OIHF), North Atlantic Current, spatiotemporal variation

Citation Liu Yuang, Wang Xiaoqiao, Ding Jinfeng, Zhang Lujun. 2025. Seasonal variations of ocean-to-ice heat flux in north of the Fram Strait, Arctic Ocean. Acta Oceanologica Sinica, 44(3): 71–83, doi: 10.1007/s13131-025-2476-2

1 Introduction

In recent years, the Arctic environment has undergone rapid changes, with a notable increase in temperature in the Arctic Ocean that is two to three times greater than the global rise due to the Arctic amplification (Nghiem et al., 2007; Lei et al., 2015; Serreze et al., 2009; Marshall et al., 2015; Pithan and Mauritsen, 2014; Huang et al., 2017; Chylek et al., 2022; Rantanen et al., 2022). The thickness of Arctic sea ice has been observed to decrease significantly since the 1980s, as evidenced by satellite datasets (Stroeve and Notz, 2018; Previdi et al., 2021; Xie et al., 2013; Rodrigues, 2008). This trend has been accompanied by a substantial reduction in the coverage of multi-year ice (Markus et al., 2009). The thinning of the ice pack will result in increased fragmentation and mobility of sea ice (Graham et al., 2019; Spreen et al., 2011), which further leads to enhanced atmosphere-ocean interaction. This, in turn, will facilitate greater ocean mixing and potentially increase the vertical heat flux in the upper ocean. The warming and sea ice loss have a significant impact on the Arctic ecosystem, and this impact are expected to intensify in the coming decades (Johannessen and Miles, 2011; Vincent et al., 2011; Fu et al., 2020; Grémillet and Descamps, 2023). Furthermore, the warming of the Arctic and the reduction of sea ice may also affect Eurasian and North American midlatitudes weather patterns (Honda et al., 2009; Francis et al., 2017; Overland et al., 2016; Blackport et al., 2019; Screen and Blackport, 2019). Consequently, the substantial decline in Arctic sea ice increased the demand for more accurate simulation and prediction of the Arctic sea ice conditions.

Ocean-to-Ice Heat Flux (OIHF) represents the transfer of heat from the ocean to the ice at the interface, and plays a pivotal role in regulating the melting and growth of sea ice (Zhong et al., 2022). In the context of significant decline in the extent and thickness of Arctic sea ice as revealed by early studies (Comiso, 2002; Rothrock et al., 2003), it is imperative to gain a comprehensive understanding of the contributions made by the OIHF. Sea ice

Foundation item: The National Natural Science Foundation of China under contract Nos 42406259, 42175172, and 41975134; the Science Foundation for Youths of Hunan Province (Category C) under contract No. 2025JJ60240.
*Corresponding author, E-mail: wangxiaoqiao23@nudt.edu.cn

concentration, mixed-layer depth and other variables or processes that affect the ocean heat content all have impacts on OIHF. For example, the winter OIHF has increased significantly as a result of the entrainment of heat from the Atlantic water into the mixed layer, due to the weakening of the halocline in the Eurasian Basin (Polyakov et al., 2020). Brine-driven surface convection has been demonstrated to drive the upward heat entrainment of Atlantic water (Polyakov et al., 2013, 2020), thereby contributing to the increase of OIHF. Additionally, OIHF variations may also be influenced by Ekman pumping, with upwelling conditions increasing the likelihood of entrainment (Dewey et al., 2018; Meneghello et al., 2018; Zhong et al., 2018).

Direct measurement of OIHF is challenging because it requires high-frequency, high-precision measurements of temperature, salinity, and vertical velocity within the near-surface boundary layer beneath drifting sea ice. Therefore, previous studies have primarily derived OIHF estimates indirectly from observational data. For example, if the melting and thickening of sea ice is assumed to be a slow process under quasi-equilibrium conditions (Perovich et al., 1989), the OIHF can be obtained through the thermal equilibrium equation. Since turbulent measurements are rare and sparse both in space and time, parametric methods can also be used to analyze the OIHF from a large-scale perspective (Zhong et al., 2022). Based on observations, previous studies have provided a basic understanding of the variability of OIHF. In the Arctic, the equilibrium ice thickness of about 3 m may be maintained by an annual average OIHF of 2 W/m^2 (Maykut, 1982; Maykut and Untersteiner, 1971). Therefore, OIHF was assumed to be constant at 2 W/m^2 in earlier studies, while later observations contradicted this assumption. For example, the seasonal variations of OIHF have been studied, with values reaching up to 60 W/m^2 in summer (Maykut and McPhee, 1995; Perovich et al., 1997) and less than 2 W/m^2 in winter (Krishfield and Perovich, 2005). Zhong et al. (2018) observed an increase in winter OIHF in the Beaufort circulation area, rising from 0.76 W/m^2 in 2006−2012 to 1.63 W/m^2 in 2013−2018. Zhong et al. (2022) further suggested that the winter increase in OIHF is primarily driven by the deepening of the mixed layer, which enhances subsurface heat entrainment and leads to higher OIHF.

During the melt season, the sea ice concentration decreases and then solar radiation enters the upper ocean through thin ice, heat is rapidly mixed and stored in the upper ocean (Krishfield and Perovich, 2005; Maykut, 1982; Maykut and McPhee, 1995; Steele et al., 2010; Timmermans, 2015; Toole et al., 2010). In summer, solar heating of the upper mixed layer is the primary source of OIHF (Krishfield and Perovich, 2005; Maykut, 1982; Maykut and McPhee, 1995; Steele et al., 2010; Timmermans, 2015; Toole et al., 2010) and thus previous studies attributed OIHF primarily to solar radiation rather than to warm water upwelling. However, some subsequent studies have elucidated the mechanisms of increased OIHF caused by winter entrainment of heat from warm water sources, such as the Atlantic or Pacific warm water (Peterson et al., 2017; Jackson et al., 2012; Steele and Morison, 1993; Yang et al., 2001). During non-melting periods, solar radiation decreases and more heat is transported from the warm deep water to the ice floor by entrainment from storm-induced upwelling. The winter ocean heat transport is influenced by mixed layer depth, sea ice concentration, ocean convection (McPhee, 1992), and Ekman upwelling. These factors show significant seasonal and interannual variations, which also strongly affect the variations of the OIHF.

The winter OIHF is largely influenced by the Pacific water or Atlantic water (Fer et al., 2017; Jackson et al., 2012; Steele and Morison, 1993; Yang et al., 2001). The Arctic Ocean is located at the north of the North Atlantic Current, where heat from the Atlantic water can enter the Arctic Ocean through the Nordic seas (Fig. 1). Atlantic water enters the Arctic Ocean through two primary inflow pathways: the Barents Sea branch transports the greatest quantity of heat to the atmosphere above the shallow continental shelves of the Barents and Kara Seas (Smedsrud et al., 2013), while the Fram Strait branch transports ocean heat to the warm layer of the Arctic Ocean (Aagaard and Carmack, 1989). Ocean heat from the Atlantic water can penetrate to the surface and induce melting of the sea ice in the Barents Sea and Greenland Sea (Carmack et al., 2015; Dmitrenko et al., 2014; Ivanov et al., 2012; Onarheim et al., 2014; Polyakov et al., 2010). Evidence suggests that Atlantic water contributes to the sea ice melting in the Greenland Sea, as indicated by significant sea ice loss in the Eurasian Basin and increased heat content of Atlantic water (Onarheim et al., 2014; Polyakov et al., 2017; Walczowski and Piechura, 2011). Nevertheless, the impact of seasonal variations in Atlantic water on the north of Fram Strait remains to be elucidated. Climate simulations for future scenarios suggest that deep convection may become widespread in the Arctic Ocean (Lique et al., 2018), potentially transporting more oceanic heat toward the sea ice.

Due to observational limitations, unresolved issues remain in the study of OIHF in the Arctic. Because direct observations are rare and sparse both in space and time, studies of continuous OIHF across different spatiotemporal scales remain limited. This study analyzes seasonal variations in climatological OIHF averaged from 1991 to 2020 based on the regional Arctic Ocean/sea ice reanalysis (RARE) 1.15.2, mainly focusing on the north of the Fram Strait (the yellow box in Fig. 1). Using the RARE product, this study provides a high-resolution OIHF analysis over a thirty-year period. Factors such as sea ice concentration, potential temperature, current velocity, and the Arctic circulation system are considered to elucidate the potential mechanisms in regulating the variation of OIHF

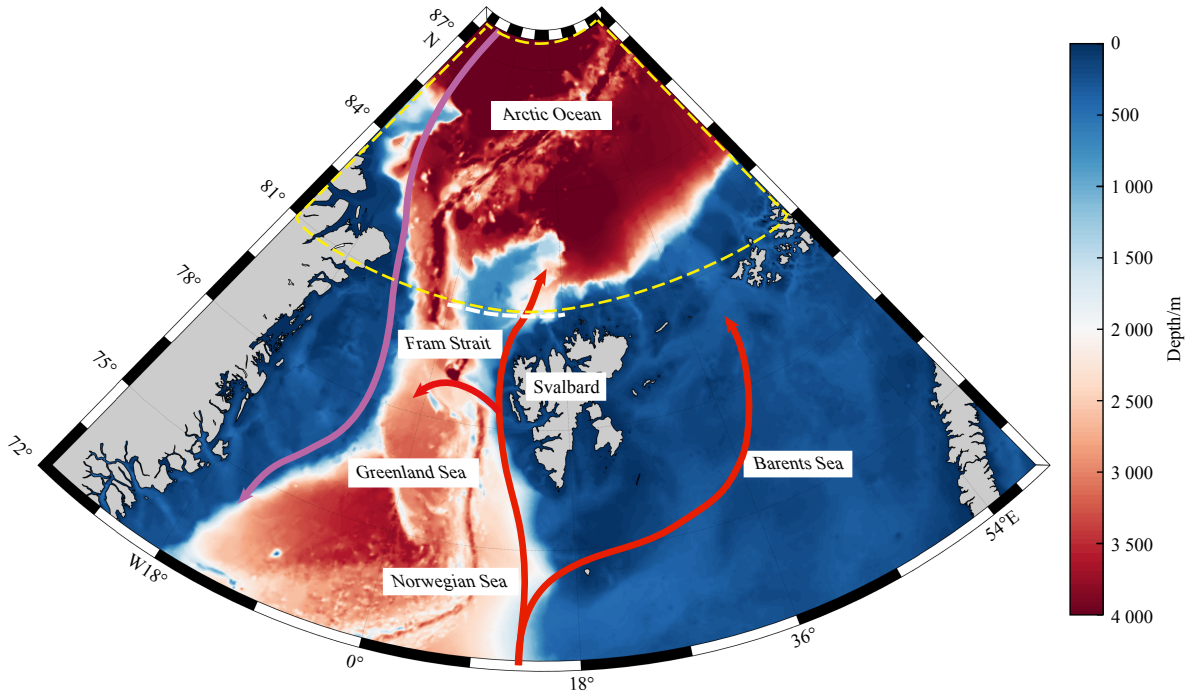


Fig. 1. Geographical distribution of topography over the Fram Strait and the surrounding region. The red and purple arrows show the approximate main pathways of the warm (Atlantic water) and cold water (transpolar drift), respectively. The yellow dashed box indicates the region of interest, while the white dashed line represents the profile analyzed in this study.

in north of the Fram Strait. Section 2 introduces the RARE reanalysis product and some methods used in this study; Section 3 presents results on the spatiotemporal variation of OIHF in north of the Fram Strait (81°−87°N, 30°W−60°E) and the oceanic factor controlling the variation in OIHF, also some discussion compared with previous researches are given; Section 4 summarizes the study.

2 Data and methods

RARE is a newly developed, high-resolution dataset designed to provide comprehensive insights into the Arctic Ocean and sea ice dynamics over a 41-year period (1980−2020). The RARE reanalysis spans the subpolar/polar cap northward of 45°N, with horizontal resolutions ranging between 2 km and 5 km and vertical resolutions between 1 m and 10 m in the upper 100 m (Carton and Chepurin, 2023). The ocean/sea ice model relies on Geophysical Fluid Dynamics Laboratory (GFDL) Modular Ocean Model (MOM5)/Sea Ice Simulator (SIS1) numerics (Winton, 2000; Griffies, 2004), while the sea ice component employs a five-layer version of the GFDL sea ice simulator version 1 for its dynamics (Carton and Chepurin, 2023). The dataset includes temporal resolutions at both 5-d and monthly intervals, capturing key oceanographic and atmospheric interactions within this climatically sensitive region.

RARE employs the same modeling and data assimilation framework as the coarser-resolution Simple Ocean Data Assimilation 3.15.2 (SODA3), developed under the simple ocean data assimilation project (Carton et al., 2018; Grodsky et al., 2024). The sequential data assimilation was conducted in RARE product to constrain temperature and salinity fields, based on the observational data from World Ocean Database, *in situ* and satellite-derived sea surface temperature, and sea ice thickness estimates from Pan-Arctic Ice-Ocean Modeling and Assimilation System (PIOMAS) (Carton and Chepurin, 2023). The improved spatial resolution of RARE has demonstrated enhanced agreement with observations, yielding stronger and more compact current structures and improved along-isopycnal heat and salt transport (Carton and Chepurin, 2023), which is substantial for the OIHF variation in the upper ocean. This higher resolution has also shown improved simulation accuracy in sea ice fields, aligning well with atmospheric forcing fields (Ge et al., 2023). RARE1.15.2 is compared to a coarser-resolution SODA3.15.2, which uses the same modeling and data assimilation system (Carton and Chepurin, 2023). The RARE dataset produces stronger more compact currents, enhances eddy kinetic energy, and strengthens along-isopycnal heat and salt transports, but reduces vertical exchanges and thus strengthens upper ocean haline stratification. Comparative analyses between RARE, SODA3, and the Hadley Centre EN4.2.2 objective analysis demonstrate that, in regions with extensive data coverage, such as the Nordic seas, the three products produce similar time-mean distributions of temperature and salinity (Carton and Chepurin, 2023). However, in areas with sparse or temporally variable data coverage, EN4.2.2 exhibits

greater sensitivity to data inhomogeneities, which may affect its accuracy in long-term climate analyses (Carton et al., 2019). Furthermore, RARE and SODA3 products enable examination of interannual temperature variability impacts from subpolar gyres on the Arctic Ocean (Carton and Chepurin, 2023). This high-resolution RARE product aims to improve documentation and deepen understanding of oceanic and sea ice dynamics within the Arctic climate system, providing valuable insights into mesoscale processes, climate feedback mechanisms, and variability (Carton and Chepurin, 2023). The SODA product has been widely used to study the global and regional ocean dynamics (e.g., Carton et al., 2005; Carton and Giese, 2008; Shenoi et al., 2005; Liu et al., 2011; Duan et al., 2013). Considering the RARE and SODA dataset use the same modeling and data assimilation system, these also lend some credibility to the RARE data and results in this work. The RARE dataset is publicly accessible at https://www2.atmos.umd.edu/~ocean/index_files/rare1.15.2_download.htm.

To provide an overview of the spatiotemporal distributions of OIHF in the Arctic Ocean, the climatological distributions of sea ice and oceanic variables are analyzed using the RARE product from 1991 to 2020. The ocean/sea ice model of RARE uses GFDL MOM5/SIS1 numerics (Carton and Chepurin, 2023; Winton, 2000; Griffies, 2004). And the sea ice model Sea Ice Simulator version 1 (SIS1) is a reformulated three-layer sea ice model. The model retains the layer structure but treats the upper half of the ice as a variable heat capacity layer. In this way, the brine reservoir is treated more physically and naturally without an increase in computational expense. It avoids double counting the melting of brine contained in the ice when ice melts at the surface. Thus, the reduction in brine that accompanies surface melting is automatically handled in the new model. A further advantage of the new model is that it is fully implicit, eliminating the need to switch to a zero-heat-capacity model when the ice becomes thin (Winton, 2000). In SIS1, the OIHF (F_b) is a linear function of the ice-ocean temperature difference (Winton, 2001) in Eq. (1), where K_o represents the heat transfer coefficient at the ice-ocean interface. T_o is the sea surface temperature, and T_f is the temperature of the ice/ocean interface which is fixed at the (salinity dependent) seawater freezing temperature.

$$F_b = K_o(T_o - T_f). \quad (1)$$

The Sea Ice Concentration (SIC) in RARE dataset was compared with that of the National Snow and Ice Data Center (NSIDC), focusing on the marginal ice zone (SIC < 0.8) as illustrated in Fig. 2. The seasonal climatological distributions of SIC in both datasets show minimal discrepancies, thereby providing a degree of validation for the accuracy of the RARE dataset.

The upper waters (0−500 m) in the Atlantic Ocean are divided into four major water masses (Emery and Meincke, 1986), including Atlantic Subarctic Upper Water, Western North Atlantic Central Water, Eastern North Atlantic Central Water, and the South Atlantic Central Water. Analysis of the water masses allows the influence of the Atlantic water on OIHF in north of the Fram Strait to be investigated. The potential temperature and salinity ranges that define the upper Atlantic waters in the North Atlantic are identified as 2.0−4.0℃ and 34.0−35.0, respectively (Emery and Meincke, 1986). The temperature-salinity (*T*-*S*) analysis was performed to illustrate the variations in water masses. The characteristics of the water masses associated with the North Atlantic Current (not shown) indicates that Atlantic water primarily accumulate at depth of 100−200 m after entering the Arctic Ocean through the Fram Strait. Therefore, subsequent analysis will focus on the core depth of Atlantic water within 100−200 m range.

3 Results and discussion

3.1 *Variation of OIHF*

The monthly climatological OIHF was averaged over 1991−2020 in the Arctic Ocean, which demonstrates that the seasonal variation of OIHF is more pronounced in the Atlantic sector compared to other regions (not shown). Therefore, the spatial distribution of OIHF in the Atlantic sector was examined to illustrate the seasonal properties. As illustrated in Fig. 3, a broad zone with high-OIHF values, extends across the latitudinal range of 72°−81°N and the longitudinal range of approximately 18°W−54°E. This high-OIHF zone exhibits notable seasonal variation in both intensity and spatial extent, reaching the maximum width and intensity during winter (December−February, Figs 3a−c). Meanwhile, a discrete region with such relatively high-OIHF values also occurs in north of the Fram Strait (81°−87°N, 30°W−60°E), reaching a maximum of 30 W/m² over the wintertime (Figs 3a−c). This region is distinct from the main broad high-OIHF zone previously mentioned. Such high-OIHF features over the northern Fram Strait is most extensive in January (Fig. 3b), gradually diminishing in February (Fig. 3c) and largely disappearing by March (Fig. 3d). During the summertime, there is a notable decline in OIHF values, with minimal heat flux observed and a reduction in the extent of the broad high-OIHF zone (June−August, Figs 3g−i). By the autumn (September−November, Figs 3j−l), the OIHF over the Norwegian Sea began to increase again. Generally, OIHF in north of the Fram Strait shows the most significant seasonal variation over the wintertime, which might be attributed to oceanic processes rather than the solar heating given the high-latitude location.

To figure out the consistency between OIHF and the SIC in north of the Fram Strait, the spatial distribution of monthly climatological SIC from 1991 to 2020 was pre-

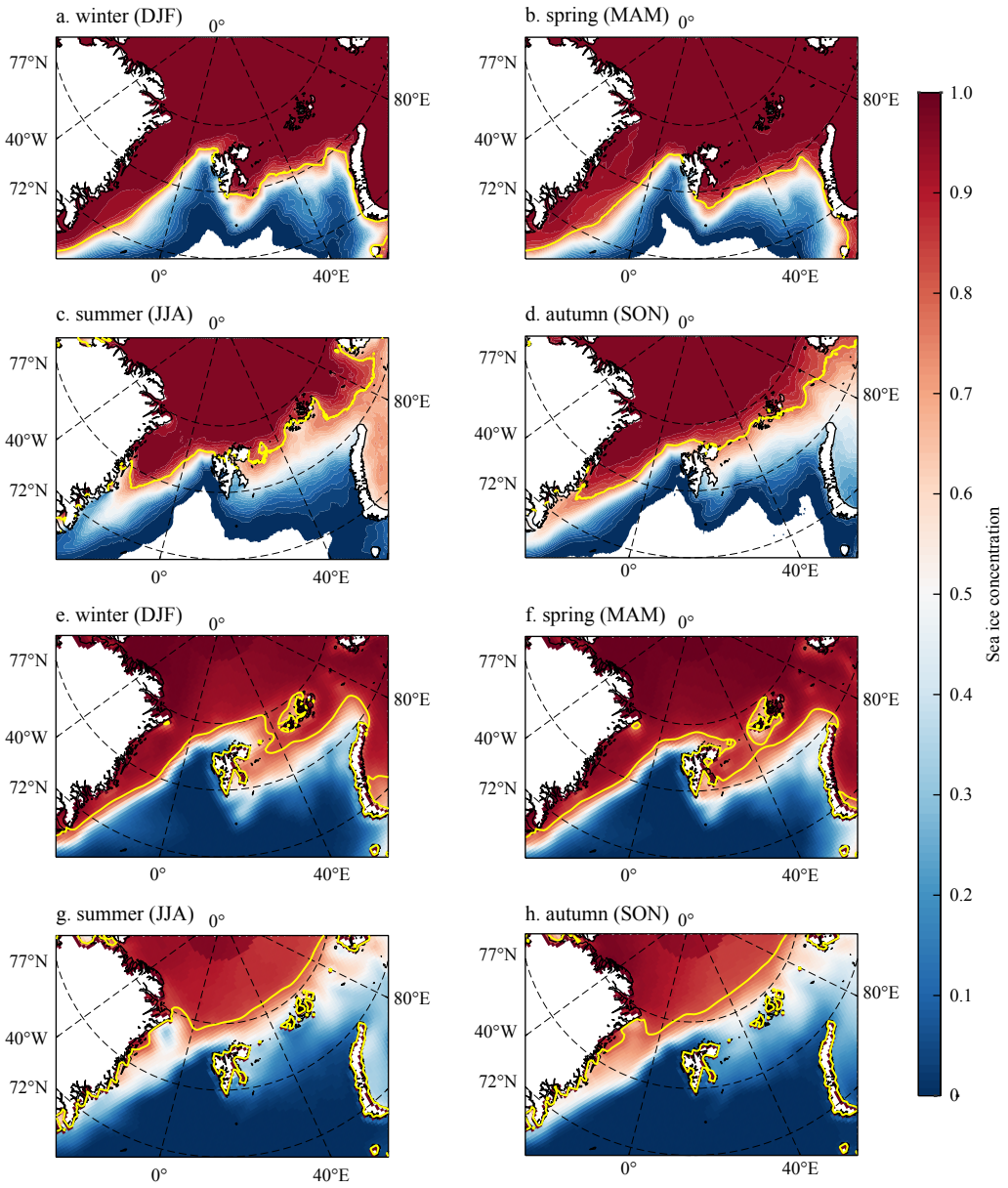


Fig. 2. Seasonal climatological distribution of sea ice concentration in RARE (a–d) and NSIDC (e–h) from 1991 to 2020, with marginal ice zones plotted in yellow lines. DJF: December–February; MAM: March–May; JJA: June–August; SON: September–November.

sented in Fig. 4. Figure 4 demonstrates that the broad high-OIHF zone identified in Fig. 3 is located within the marginal ice zone, where the SIC is relatively low, particularly south of 78°N. In such low-SIC area, the penetration of solar radiation could increase, which can further enhance the subsurface heat entrainment and finally induce such high-OIHF at the ice-ocean interface. This interaction highlights a positive feedback over the low-SIC region: such higher OIHF occurs result from the enhanced heat entrainment and solar radiation absorption, which could further reduce SIC by melting sea ice. Meanwhile, as sea ice melts, additional solar radiation penetrates into the ocean, increasing oceanic heat content and sustaining the upward heat flux. The high OIHF values observed during winter are typically associated with high SIC (Figs 4a–c), usually along with thick ice cover. Under the harsh sea ice conditions in north of the Fram Strait, the influence of solar radiation on OIHF is minimal, and the local atmospheric processes are unable to affect the OIHF by enhancing ocean mixing or convection. Based on these results, we hypothesized that the increased OIHF values may primarily arise from the intrusion of warmer waters into this region, such as the transport of Atlantic warm water. To further investigate the potential processes driving these high OIHF values, we then examined the temporal variation of potential temperature in north of the Fram Strait (Fig. 5).

Figure 5 presents the monthly climatological distribution of average potential temperature at depth of 100–200 m over 1991–2020. This depth range was selected as

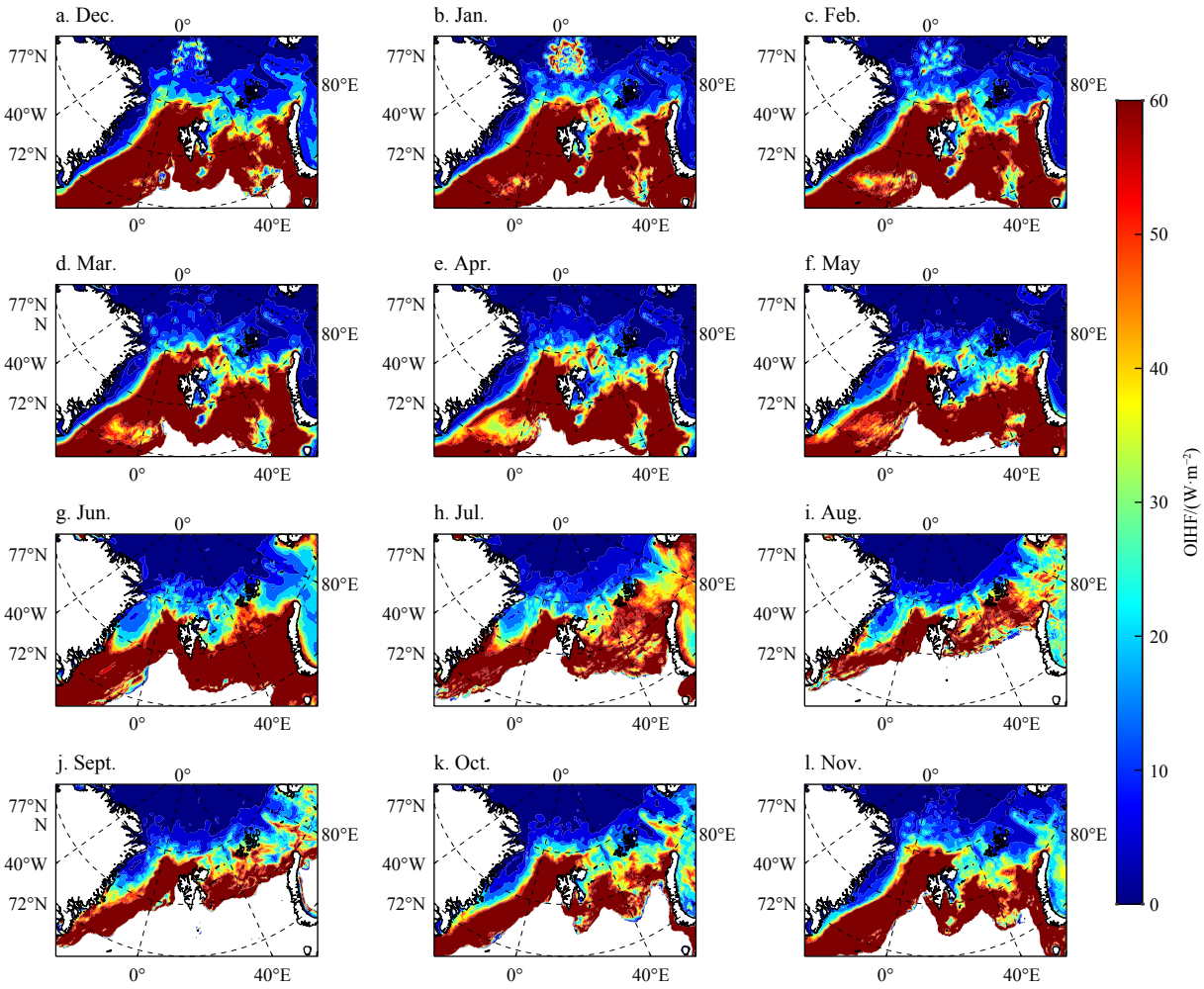


Fig. 3. Monthly climatological distribution of ocean-to-ice heat flux (OIHF) from 1991 to 2020.

it represents the core layer of relatively warm Atlantic water, as described in Section 2. By focusing on this depth, we aim to capture the spatial distribution of the primary heat source in north of the Fram Strait. Figure 5 reveals a distinct region of high potential temperature extending from the North Atlantic Ocean to the Fram Strait, consistent with the positions of the two primary pathways of warm Atlantic water shown in Fig. 1. This pattern suggests that the temperature distribution effectively reflects the transport of Atlantic water. During spring and summer, warm waters reach up to approximately 82°N, with little to no warm water signal further north, such as in the Nansen Basin, north of the Fram Strait (Figs 5e–j). However, in autumn and winter, these warm waters extend into the north of the Fram Strait (Figs 5a–d and k–l), suggesting a potential seasonal heat transport from the North Atlantic Ocean.

The averaged potential temperature distribution indicates that the water in north of the Fram Strait reaches its highest temperatures in winter (Figs 5a–c), which is consistent with the notable increase in OIHF values observed during the same period (Figs 3a–c). Further examination reveals that potential temperatures in this region begin to rise in October (Fig. 5k), and remain elevated through February and March (Figs 5c–d). However, when examining the monthly distribution of OIHF (Fig. 3), high OIHF values in north of the Fram Strait primarily begin in December (Fig. 3l), reaching the peak in January (Fig. 3b), and start to weaken by February (Fig. 3c). This suggests that changes in subsurface temperature may exert a cumulative lag effect on the OIHF. The most significant impact on the OIHF occurs approximately 2–3 months after the sustained increase in potential temperature of the subsurface layer. Therefore, we conclude that the extreme high-OIHF values in winter are primarily driven by the intrusion of Atlantic waters, which raises subsurface temperatures and subsequently enhances the heat flux at the ice-ocean interface. Based on this, we further quantified the characteristics and volume transport of Atlantic water in subsequent analyses.

3.2 *Atlantic inflow*

The northward inflow of Atlantic water is a key component of the Atlantic meridional overturning circulation, driven by thermohaline convection (Ganachaud and Wunsch, 2000), and transports warm Atlantic water toward the surface in the northern regions (Aagaard, 1989). To examine the spatiotemporal variations of the North Atlantic

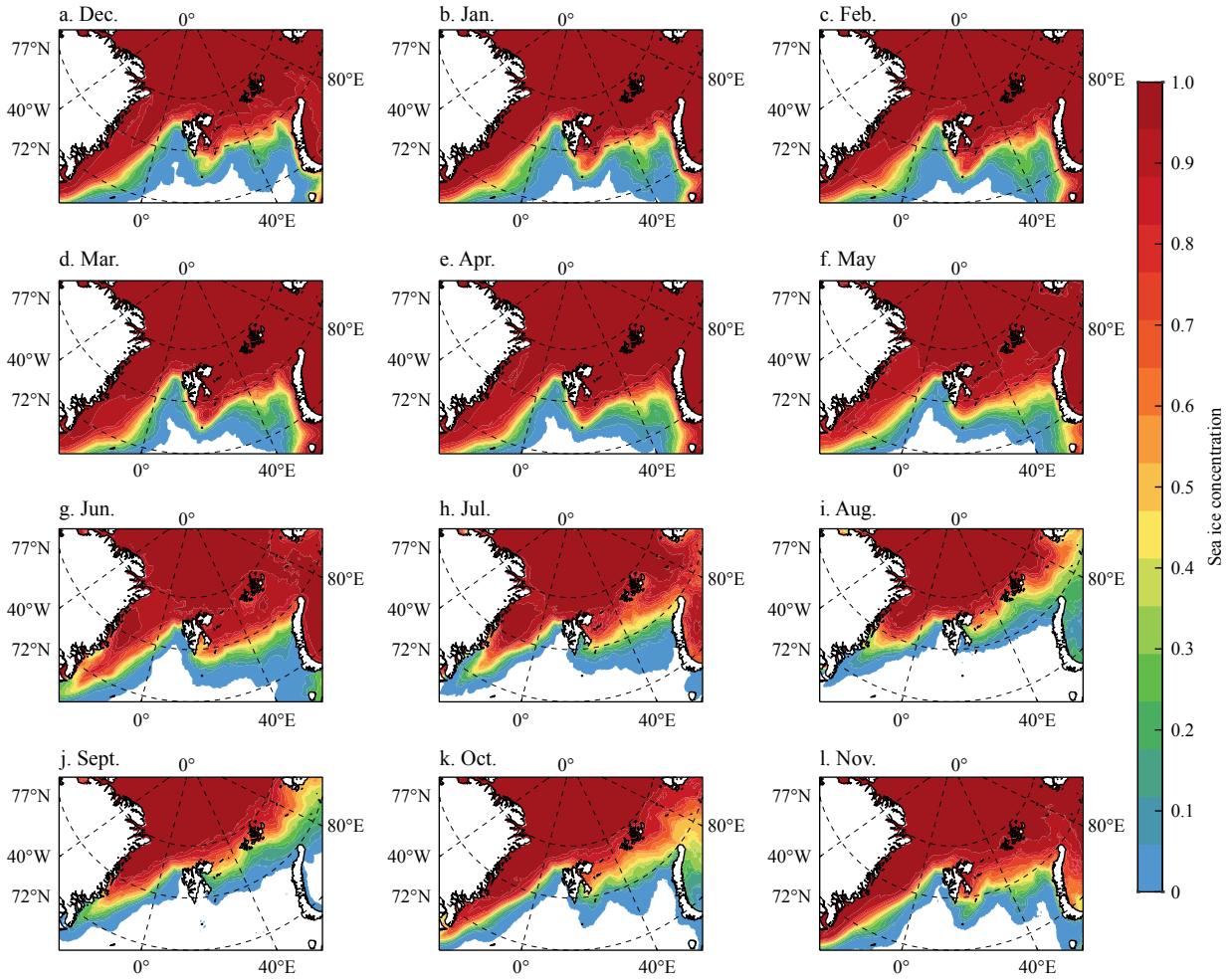


Fig. 4. Monthly climatological distribution of sea ice concentration from 1991 to 2020.

Current, we focused on the north of the Fram Strait (81°−87°N, 30°W−60°E), indicated by the yellow box in Fig. 1, where winter OIHF increased apparently (Fig. 3). The analysis centers on the water masses within the core depth range of 100−200 m. Monthly climatological *T*-*S* diagram for the north of the Fram Strait is shown in Fig. 6. The colorbar represents the proportion of grid points within each *T*-*S* unit relative to the total number of grid points. The *T*-*S* range for Atlantic water is outlined by a red box (Fig. 6), highlighting the intrusion of Atlantic water into the north of the Fram Strait. It is evident that during winter, the proportion of Atlantic water significantly increases over the entire region (Figs 6a−c), indicating a substantial intrusion of warm Atlantic water into the north of the Fram Strait. This is consistent with the potential temperature increase observed earlier (Figs 5a−c). Furthermore, the *T*-*S* diagram shows that from October onward (Fig. 6k), the proportion of Atlantic water gradually rises, reaching its peak around January and February (Figs 6b−c), after which it decreases during spring and summer (Figs 6d−j). These findings align closely with the spatial distribution and temporal changes in potential temperature shown in Fig. 5, indicating that the intrusion of this warm water mass directly influences the subsurface temperature distribution.

To better understand the vertical intrusion characteristics of Atlantic water, we presented the distribution of potential temperature within the latitudinal range of significant OIHF variation along the 0° meridian (82°−88°N). As expected, during the winter months, a pronounced warm signal is observed, gradually extending northward, with warm water exceeding 1℃ penetrating up to depths smaller than 100 m (Figs 7a−c), thereby significantly influencing OIHF (Figs 3a−c). This vertical seasonal variation is consistent with the changes in the proportion of water masses shown in Fig. 6, clearly demonstrating that the water mass intrusion begins to intensify in October (Figs 6k and 7k). The warm water signal progressively extends both northward and upward, reaching its peak intensity in late winter (Figs 7b−c), weakening during spring (Figs 7d−f), and becoming weakest in summer (Figs 7g−i).

3.3 *Relationship between OIHF and the Atlantic inflow*

Based on the analysis of spatiotemporal variations in OIHF over the north of the Fram Strait in Sections 3.1 and 3.2, it is concluded that the notable increase in OIHF is

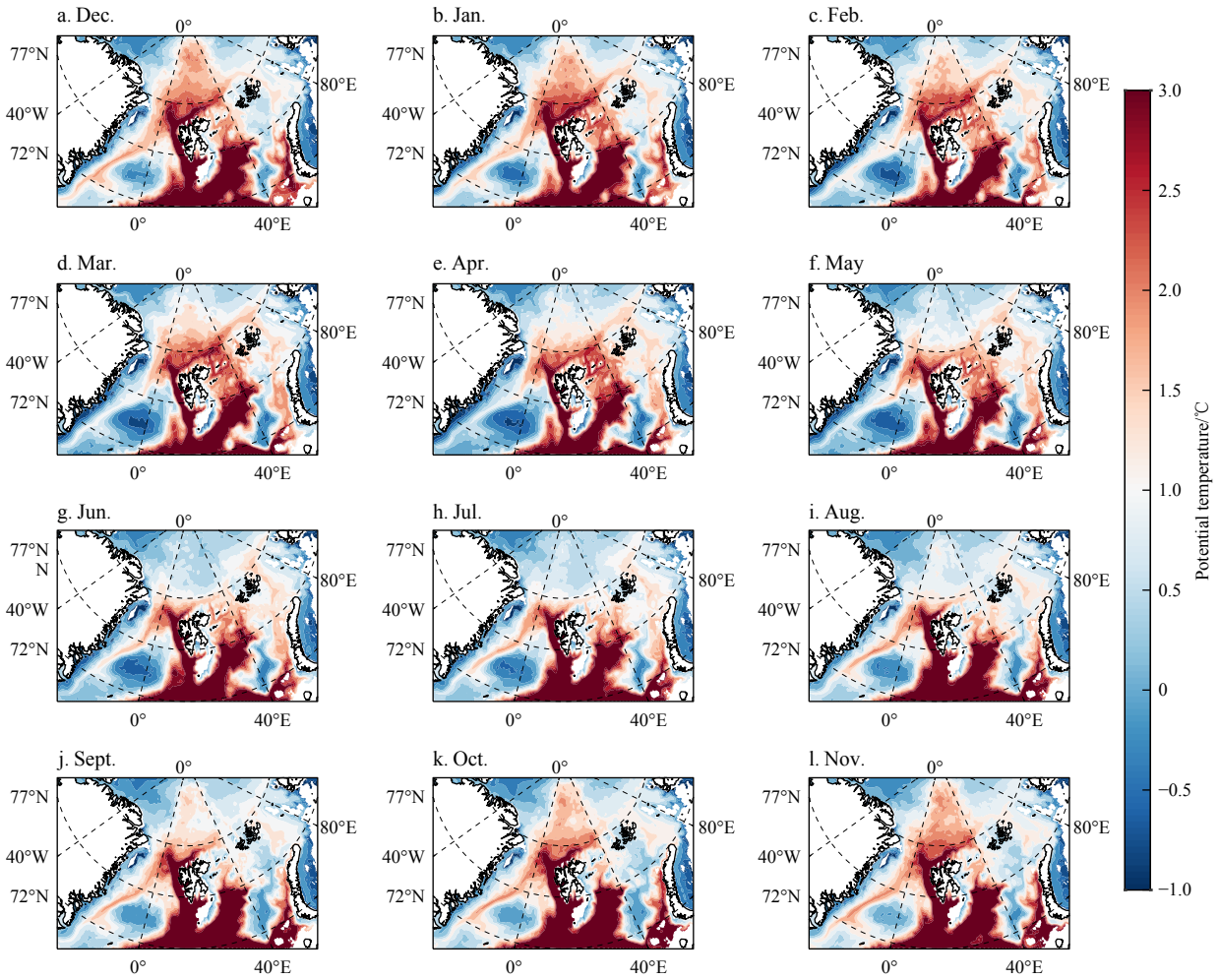


Fig. 5. Monthly climatological distribution of average potential temperature at the depth of 100−200 m from 1991 to 2020.

primarily driven by enhanced heat transport from the North Atlantic Current during winter. To further investigate this relationship, the correlation between OIHF and volume transport of Atlantic water was examined in this section. Spatial averaged climatological OIHF were calculated over the north of the Fram Strait (81°−87°N, 30°W−60°E, indicated by the yellow dashed box in Fig. 1). Additionally, the monthly climatological volume transport of Atlantic water across the defined transect (shown as the white dashed line in Fig. 1) was quantified. Figure 8 shows the time series of OIHF and Atlantic water transport, which exhibits clear seasonal variations, reaching a minimum in summer and a maximum in winter. The peak in the spatial averaged OIHF occurs in January, with a significant increase beginning in October (Fig. 8). The correlation coefficient and p-value (r = 0.86, $P < 0.001$) indicate a strong positive correlation between the OIHF and volume transport of Atlantic water. These results further emphasize the relationship between the seasonal variations of OIHF and the North Atlantic Current system. The seasonal variation in Atlantic water intrusion into the Arctic Ocean can be partially attributed to the seasonal fluctuations in Arctic strong cyclones (Liu and He, 2023). During the winter months, both the frequency and intensity of these cyclones increase (Liu and He, 2023), which in turn enhance the potential vorticity of the North Atlantic Current, thereby facilitating further transport of Atlantic water into the Arctic Ocean. These cyclones also influence the subsurface and upper ocean layers through vertical mixing (Liu and He, 2023). The mixing and intrusion processes driven by Arctic cyclones disrupt the stable stratification of the ocean, reducing subsurface ocean density and the buoyancy frequency. This disruption accelerates the northward intrusion of Atlantic water, increasing subsurface ocean heat content and promoting mixing between warm Atlantic water and colder Arctic water. As a result, these processes contribute to an increase in ocean heat content and facilitate Atlantification in the Arctic Ocean. Previous studies have also examined the intrusion of the North Atlantic Current into the north of Svalbard, similar to the focus of this study (Duarte et al., 2020). However, their analysis primarily centered on sea ice melt rather than OIHF, and they did not account for the seasonal variations of the North Atlantic Current, which play a significant role in influencing winter sea ice dynamics.

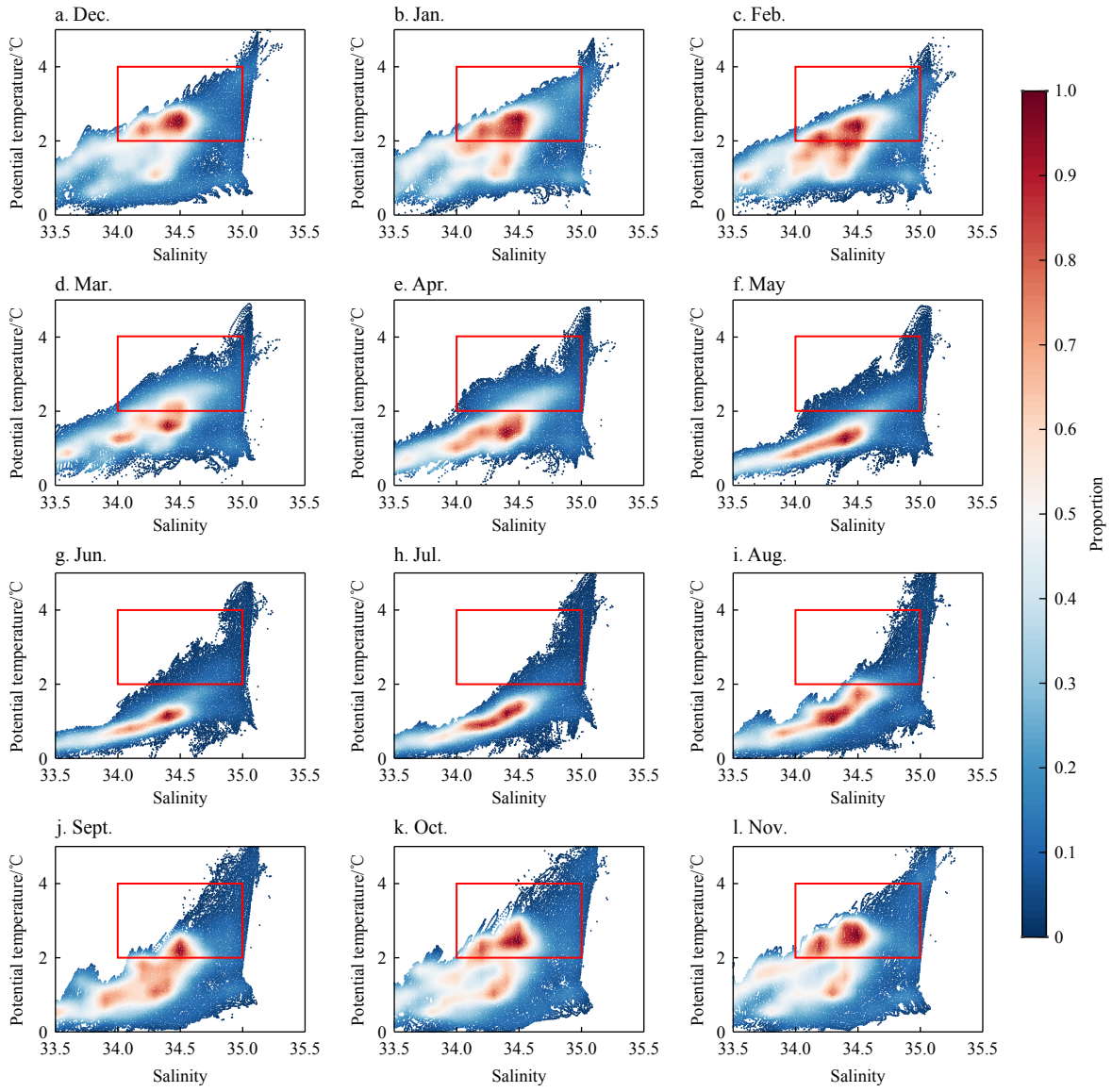


Fig. 6. Monthly climatological temperature-salinity diagram at the depth of 100–200 m in the north of the Fram Strait from 1991 to 2020. Color represents the proportion of water masses, and red boxes indicate Atlantic water.

4 Conclusions

This paper investigates the seasonal variations and driving mechanisms of OIHF over north of the Fram Strait and the surrounding regions using the high-resolution RARE dataset from 1991 to 2020. The results show that the OIHF exhibits significant spatiotemporal variability, with a belt-shaped region of high heat flux in the marginal ice zone. This region reaches its maximum width and intensity during winter, especially in north of the Fram Strait. Analysis of potential temperature and salinity reveals that the proportion of Atlantic water in north of the Fram Strait increases significantly during winter. This warm water intrusion begins in October, peaks in January and February, and then decreases during spring and summer. The enhanced presence of Atlantic water raises subsurface temperatures, which, combined with the northward heat transport, drives the observed winter peaks in OIHF. The warming in subsurface layers also leads to a lagged response in the OIHF, with a delay of about 2−3 months. Furthermore, vertical distributions of potential temperature also reveal a clear seasonal pattern, with warm Atlantic waters penetrating northward and upward during winter. This significantly reduces ocean stratification and promotes vertical heat transport, further intensifying OIHF. The strong correlation between OIHF and the volume transport of Atlantic water shows that the seasonal peak in OIHF is driven by increased inflows of Atlantic water during winter.

Overall, this study highlights the critical role of the North Atlantic Current and its seasonal dynamics in shaping variations in OIHF and their impacts on Arctic sea ice. Future research should focus on understanding the drivers of these seasonal variations, particularly the role of Arctic cyclones and their interactions with oceanic processes. Additionally, detailed heat budget analyses are necessary

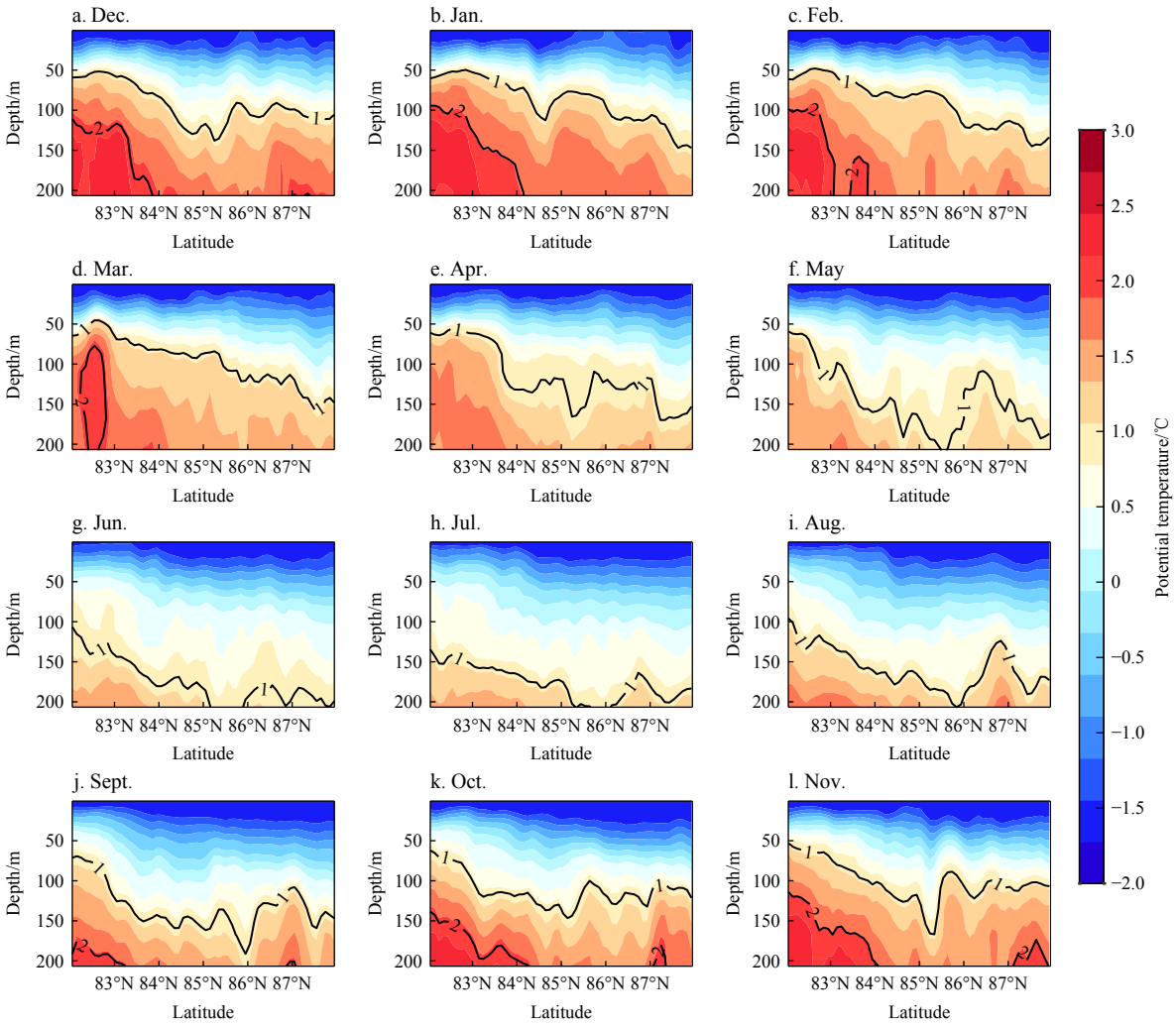


Fig. 7. Vertical transects of monthly climatological potential temperature at 0° meridian over the north of the Fram Strait from 1991 to 2020. The black lines represent the isobars of potential temperature at 1℃ or 2℃.

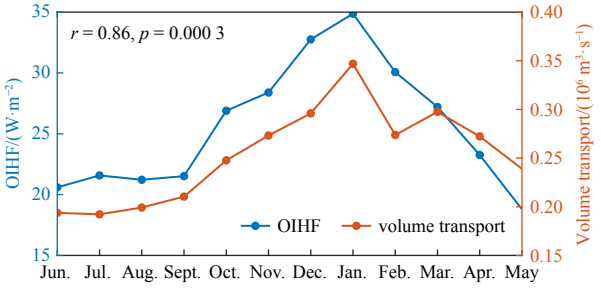


Fig. 8. Time series of monthly climatological ocean-to-ice heat flux (OIHF) and Atlantic water volume transport over the north of the Fram Strait (indicated by the yellow dashed box in Fig. 1) from 1991 to 2020.

to further quantify the contributions of OIHF to sea ice changes in north of the Fram Strait, which is essential for improving predictions of Arctic sea ice dynamics in a warming climate.

Acknowledgement

We thank the RARE (https://www2.atmos.umd.edu/~ocean/index_files/rare1.15.2_download.htm) and NSIDC (https://n5eil01u.ecs.nsidc.org/PM/NSIDC-0051.002/) for providing a suite of high-resolution reanalysis products and satellite data.

References

Aagaard K. 1989. A synthesis of the Arctic Ocean circulation. Rapports et procès-verbaux des réunions, 188: 11–22. Journal of Geophysical Research, 96: 20433–20441

Aagaard K, Carmack E C. 1989. The role of sea ice and other fresh water in the Arctic circulation. Journal of Geophysical Research: Oceans, 94(C10): 14485–14498, doi: 10.1029/JC094iC10p14485

Blackport R, Screen J A, Van Der Wiel K, et al. 2019. Minimal influence of reduced Arctic sea ice on coincident cold winters in mid-latitudes. Nature Climate Change, 2019(9): 697–704, doi: 10.1038/s41558-019-0551-4

Carmack E, Polyakov I, Padman L, et al. 2015. Toward quantifying the increasing role of oceanic heat in sea ice loss in the new Arctic. Bulletin of the American Meteorological

Society, 96(12): 2079–2105, doi: 10.1175/BAMS-D-13-00177.1

Carton J A, Chepurin G A. 2023. RARE: The regional Arctic reanalysis. Journal of Climate, 36(8): 2333–2348, doi: 10.1175/JCLI-D-22-0340.1

Carton J A, Chepurin G A, Chen L G. 2018. SODA3: A new ocean climate reanalysis. Journal of Climate, 31(17): 6967–6983, doi: 10.1175/JCLI-D-18-0149.1

Carton J A, Giese B S. 2008. A reanalysis of ocean climate using simple ocean data assimilation (SODA). Monthly Weather Review, 136(8): 2999–3017, doi: 10.1175/2007MWR1978.1

Carton J A, Giese B S, Grodsky S A. 2005. Sea level rise and the warming of the oceans in the Simple Ocean Data Assimilation (SODA) ocean reanalysis. Journal of Geophysical Research: Oceans, 110(C9): C09006

Carton J A, Penny S G, Kalnay E. 2019. Temperature and salinity variability in the SODA3, ECCO4r3, and ORAS5 ocean reanalyses, 1993–2015. Journal of Climate, 32(8): 2277–2293, doi: 10.1175/JCLI-D-18-0605.1

Chylek P, Folland C, Klett J D, et al. 2022. Annual mean Arctic amplification 1970–2020: Observed and simulated by CMIP6 climate models. Geophysical Research Letters, 49(13): e2022GL099371, doi: 10.1029/2022GL099371

Comiso J C. 2002. A rapidly declining perennial sea ice cover in the Arctic. Geophysical Research Letters, 29(20): 1956

Dewey S, Morison J, Kwok R, et al. 2018. Arctic ice-ocean coupling and gyre equilibration observed with remote sensing. Geophysical Research Letters, 45(3): 1499–1508, doi: 10.1002/2017GL076229

Dmitrenko I A, Kirillov S A, Serra N, et al. 2014. Heat loss from the Atlantic water layer in the northern Kara Sea: Causes and consequences. Ocean Science, 10(4): 719–730, doi: 10.5194/os-10-719-2014

Duan Yongliang, Hou Yijun, Liu Hongwei, et al. 2013. The water mass variability and southward shift of the Southern Hemisphere mid-depth supergyre. Acta Oceanologica Sinica, 32(11): 74–81, doi: 10.1007/s13131-013-0380-7

Duarte P, Sundfjord A, Meyer A, et al. 2020. Warm Atlantic water explains observed sea ice melt rates north of Svalbard. Journal of Geophysical Research: Oceans, 125(8): e2019JC015662, doi: 10.1029/2019JC015662

Emery W J, Meincke J. 1986. Global water masses: summary and review. Oceanologica Acta, 9(4): 383–391

Fer I, Peterson A K, Randelhoff A, et al. 2017. One-dimensional evolution of the upper water column in the Atlantic sector of the Arctic Ocean in winter. Journal of Geophysical Research: Oceans, 122(3): 1665–1682, doi: 10.1002/2016JC012431

Francis J A, Vavrus S J, Cohen J. 2017. Amplified Arctic warming and mid-latitude weather: New perspectives on emerging connections. WIREs Climate Change, 8(5): e474, doi: 10.1002/wcc.474

Fu Weiwei, Moore J K, Primeau F W, et al. 2020. A growing freshwater lens in the Arctic Ocean with sustained climate warming disrupts marine ecosystem function. Journal of Geophysical Research: Biogeosciences, 125(12): e2020JG005693, doi: 10.1029/2020JG005693

Ganachaud A, Wunsch C. 2000. Improved estimates of global ocean circulation, heat transport and mixing from hydrographic data. Nature, 408(6811): 453–457, doi: 10.1038/35044048

Ge Zhicheng, Wang Xuezhu, Wang Xidong. 2023. Evaluation of the Arctic sea-ice simulation on SODA3 datasets. Advances in Atmospheric Sciences, 40(12): 2302–2317, doi: 10.1007/s00376-023-2320-6

Graham R M, Itkin P, Meyer A, et al. 2019. Winter storms accelerate the demise of sea ice in the Atlantic sector of the Arctic Ocean. Scientific Reports, 9(1): 9222, doi: 10.1038/s41598-019-45574-5

Grémillet D, Descamps S. 2023. Ecological impacts of climate change on Arctic marine megafauna. Trends in Ecology & Evolution, 38(8): 773–783

Griffies S M. 2004. Fundamentals of Ocean Climate Models. Princeton: Princeton University Press, 528

Grodsky S A, Reul N, Vandemark D. 2024. Summer Chukchi Sea near-surface salinity variability in satellite observations and ocean models. Remote Sensing, 16(18): 3397, doi: 10.3390/rs16183397

Honda M, Inoue J, Yamane S. 2009. Influence of low Arctic sea-ice minima on anomalously cold Eurasian winters. Geophysical Research Letters, 36(8): L08707

Huang Jianbin, Zhang Xiangdong, Zhang Qiyi, et al. 2017. Recently amplified Arctic warming has contributed to a continual global warming trend. Nature Climate Change, 7(12): 875–879, doi: 10.1038/s41558-017-0009-5

Ivanov V V, Alexeev V A, Repina I, et al. 2012. Tracing Atlantic water signature in the Arctic sea ice cover east of Svalbard. Advances in Meteorology, 2012: 201818

Jackson J M, Williams W J, Carmack E C. 2012. Winter sea-ice melt in the Canada Basin, Arctic Ocean. Geophysical Research Letters, 39(3): L03603

Johannessen O M, Miles M W. 2011. Critical vulnerabilities of marine and sea ice-based ecosystems in the high Arctic. Regional Environmental Change, 11(1): 239–248

Krishfield R A, Perovich D K. 2005. Spatial and temporal variability of oceanic heat flux to the Arctic ice pack. Journal of Geophysical Research: Oceans, 110(C7): C07021

Lei Ruibo, Xie Hongjie, Wang Jia, et al. 2015. Changes in sea ice conditions along the Arctic Northeast Passage from 1979 to 2012. Cold Regions Science and Technology, 119: 132–144, doi: 10.1016/j.coldregions.2015.08.004

Lique C, Johnson H L, Plancherel Y. 2018. Emergence of deep convection in the Arctic Ocean under a warming climate. Climate Dynamics, 50(9): 3833–3847

Liu Yujun, He Yijun. 2023. Cold season Arctic strong cyclones enhance Atlantification of the Arctic Ocean. Environmental Research Letters, 18(11): 114049, doi: 10.1088/1748-9326/ad0518

Liu Hongwei, Zhang Qilong, Duan Yongliang, et al. 2011. The three-dimensional structure and seasonal variation of the North Pacific meridional overturning circulation. Acta

Oceanologica Sinica, 30(3): 33–42, doi: 10.1007/s13131-011-0117-4

Markus T, Stroeve J C, Miller J. 2009. Recent changes in Arctic sea ice melt onset, freezeup, and melt season length. Journal of Geophysical Research: Oceans, 114(C12): C12024

Marshall J, Scott J R, Armour K C, et al. 2015. The ocean's role in the transient response of climate to abrupt greenhouse gas forcing. Climate Dynamics, 44(7): 2287–2299

Maykut G A. 1982. Large-scale heat exchange and ice production in the central Arctic. Journal of Geophysical Research: Oceans, 87(C10): 7971–7984, doi: 10.1029/JC087iC10p07971

Maykut G A, McPhee M G. 1995. Solar heating of the Arctic mixed layer. Journal of Geophysical Research: Oceans, 100(C12): 24691–24703, doi: 10.1029/95JC02554

Maykut G A, Untersteiner N. 1971. Some results from a time-dependent thermodynamic model of sea ice. Journal of Geophysical Research, 76(6): 1550–1575, doi: 10.1029/JC076i006p01550

McPhee M G. 1992. Turbulent heat flux in the upper ocean under sea ice. Journal of Geophysical Research: Oceans, 97(C4): 5365–5379, doi: 10.1029/92JC00239

Meneghello G, Marshall J, Timmermans M L, et al. 2018. Observations of seasonal upwelling and downwelling in the Beaufort Sea mediated by sea ice. Journal of Physical Oceanography, 48(4): 795–805, doi: 10.1175/JPO-D-17-0188.1

Nghiem S V, Rigor I G, Perovich D K, et al. 2007. Rapid reduction of Arctic perennial sea ice. Geophysical Research Letters, 34(19): L19504

Onarheim I H, Smedsrud L H, Ingvaldsen R B, et al. 2014. Loss of sea ice during winter north of Svalbard. Tellus A: Dynamic Meteorology and Oceanography, 66(1): 23933, doi: 10.3402/tellusa.v66.23933

Overland J E, Dethloff K, Francis J A, et al. 2016. Nonlinear response of mid-latitude weather to the changing Arctic. Nature Climate Change, 6(11): 992–999, doi: 10.1038/nclimate3121

Perovich D K, Elder B C, Richter-Menge J A. 1997. Observations of the annual cycle of sea ice temperature and mass balance. Geophysical Research Letters, 24(5): 555–558, doi: 10.1029/97GL00185

Perovich D K, Tucker W B, Krishfield R A. 1989. Oceanic heat flux in the Fram Strait measured by a drifting buoy. Geophysical Research Letters, 16(9): 995–998, doi: 10.1029/GL016i009p00995

Peterson A K, Fer I, McPhee M G, et al. 2017. Turbulent heat and momentum fluxes in the upper ocean under Arctic sea ice. Journal of Geophysical Research: Oceans, 122(2): 1439–1456, doi: 10.1002/2016JC012283

Pithan F, Mauritsen T. 2014. Arctic amplification dominated by temperature feedbacks in contemporary climate models. Nature Geoscience, 7(3): 181–184, doi: 10.1038/ngeo2071

Polyakov I V, Pnyushkov A V, Alkire M B, et al. 2017. Greater role for Atlantic inflows on sea-ice loss in the Eurasian Basin of the Arctic Ocean. Science, 356(6335): 285–291, doi: 10.1126/science.aai8204

Polyakov I V, Pnyushkov A V, Rember R, et al. 2013. Winter convection transports Atlantic water heat to the surface layer in the eastern Arctic Ocean. Journal of Physical Oceanography, 43(10): 2142–2155, doi: 10.1175/JPO-D-12-0169.1

Polyakov I V, Rippeth T P, Fer I, et al. 2020. Weakening of cold halocline layer exposes sea ice to oceanic heat in the eastern Arctic Ocean. Journal of Climate, 33(18): 8107–8123, doi: 10.1175/JCLI-D-19-0976.1

Polyakov I V, Timokhov L A, Alexeev V A, et al. 2010. Arctic Ocean warming contributes to reduced polar ice cap. Journal of Physical Oceanography, 40(12): 2743–2756, doi: 10.1175/2010JPO4339.1

Previdi M, Smith K L, Polvani L M. 2021. Arctic amplification of climate change: A review of underlying mechanisms. Environmental Research Letters, 16(9): 093003, doi: 10.1088/1748-9326/ac1c29

Rantanen M, Karpechko A Y, Lipponen A, et al. 2022. The Arctic has warmed nearly four times faster than the globe since 1979. Communications Earth & Environment, 3: 168

Rodrigues J. 2008. The rapid decline of the sea ice in the Russian Arctic. Cold Regions Science and Technology, 54(2): 124–142, doi: 10.1016/j.coldregions.2008.03.008

Rothrock D A, Zhang J, Yu Y. 2003. The Arctic ice thickness anomaly of the 1990s: A consistent view from observations and models. Journal of Geophysical Research: Oceans, 108(C3): 3083

Screen J A, Blackport R. 2019. How robust is the atmospheric response to projected Arctic Sea ice loss across climate models?. Geophysical Research Letters, 46(20): 11406–11415, doi: 10.1029/2019GL084936

Serreze M C, Barrett A P, Stroeve J C, et al. 2009. The emergence of surface-based Arctic amplification. The Cryosphere, 3(1): 11–19, doi: 10.5194/tc-3-11-2009

Shenoi S S C, Shankar D, Shetye S R. 2005. On the accuracy of the simple ocean data assimilation analysis for estimating heat budgets of the near-surface Arabian Sea and Bay of Bengal. Journal of Physical Oceanography, 35(3): 395–400, doi: 10.1175/JPO-2678.1

Smedsrud L H, Esau I, Ingvaldsen R B, et al. 2013. The role of the Barents Sea in the Arctic climate system. Reviews of Geophysics, 51(3): 415–449, doi: 10.1002/rog.20017

Spreen G, Kwok R, Menemenlis D. 2011. Trends in Arctic sea ice drift and role of wind forcing: 1992–2009. Geophysical Research Letters, 38(19): L19501

Steele M, Morison J H. 1993. Hydrography and vertical fluxes of heat and salt northeast of Svalbard in autumn. Journal of Geophysical Research: Oceans, 98(C6): 10013–10024, doi: 10.1029/93JC00937

Steele M, Zhang Jinlun, Ermold W. 2010. Mechanisms of summertime upper Arctic Ocean warming and the effect on sea ice melt. Journal of Geophysical Research: Oceans, 115(C11): C11004

Stroeve J, Notz D. 2018. Changing state of Arctic sea ice across

all seasons. Environmental Research Letters, 13(10): 103001, doi: 10.1088/1748-9326/aade56

Timmermans M L. 2015. The impact of stored solar heat on Arctic sea ice growth. Geophysical Research Letters, 42(15): 6399–6406, doi: 10.1002/2015GL064541

Toole J M, Timmermans M L, Perovich D K, et al. 2010. Influences of the ocean surface mixed layer and thermohaline stratification on Arctic sea ice in the central Canada Basin. Journal of Geophysical Research: Oceans, 115(C10): C10018

Vincent W F, Callaghan T V, Dahl-Jensen D, et al. 2011. Ecological implications of changes in the Arctic cryosphere. AMBIO, 40(1): 87–99

Walczowski W, Piechura J. 2011. Influence of the West Spitsbergen Current on the local climate. International Journal of Climatology, 31(7): 1088–1093, doi: 10.1002/joc.2338

Winton M. 2000. A reformulated three-layer sea ice model. Journal of Atmospheric and Oceanic Technology, 17(4): 525–531, doi: 10.1175/1520-0426(2000)017<0525:ARTLSI>2.0.CO;2

Winton M. 2001. FMS Sea Ice Simulator. GFDL Technical Document. https://citeseerx.ist.psu.edu/document?repid=rep1&type=pdf&tdoi=f655a308717f70f8250a145ec898cf6c1b3cc7ce [2001-11-30]/[2024-10-01]

Xie H, Lei R, Ke C, et al. 2013. Summer sea ice characteristics and morphology in the Pacific Arctic sector as observed during the CHINARE 2010 cruise. The Cryosphere, 7(4): 1057–1072, doi: 10.5194/tc-7-1057-2013

Yang Jiayan, Comiso J, Krishfield R, et al. 2001. Synoptic storms and the development of the 1997 warming and freshening event in the Beaufort Sea. Geophysical Research Letters, 28(5): 799–802, doi: 10.1029/2000GL011896

Zhong Wenli, Cole S T, Zhang Jinlun, et al. 2022. Increasing winter ocean-to-ice heat flux in the Beaufort gyre region, Arctic Ocean over 2006–2018. Geophysical Research Letters, 49(2): e2021GL096216, doi: 10.1029/2021GL096216

Zhong Wenli, Steele M, Zhang Jinlun, et al. 2018. Greater role of geostrophic currents in Ekman dynamics in the western Arctic Ocean as a mechanism for Beaufort Gyre stabilization. Journal of Geophysical Research: Oceans, 123(1): 149–165, doi: 10.1002/2017JC013282